

pubs.acs.org/est Article

Controlling Arsenic Mobilization during Managed Aquifer Recharge: The Role of Sediment Heterogeneity

Sarah Fakhreddine, Henning Prommer, Steven M. Gorelick, Jason Dadakis, and Scott Fendorf*



Cite This: Environ. Sci. Technol. 2020, 54, 8728-8738



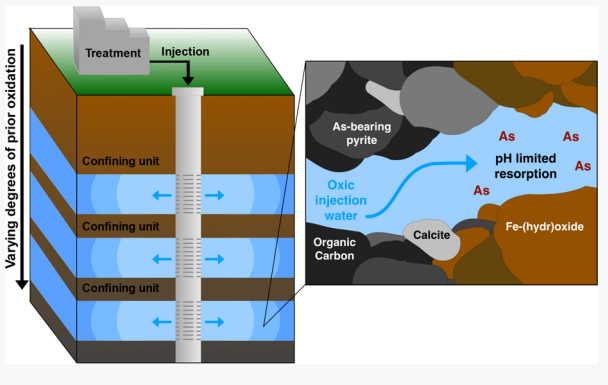
ACCESS

III Metrics & More

Article Recommendations

s Supporting Information

ABSTRACT: Managed aquifer recharge (MAR) enhances freshwater security and augments local groundwater supplies. However, geochemical and hydrological shifts during MAR can release toxic, geogenic contaminants from sediments to groundwater, threatening the viability of MAR as a water management strategy. Using reactive transport modeling coupled with aquifer analyses and measured water chemistry, we investigate the causal mechanisms of arsenic release during MAR via injection in the Orange County Groundwater Basin. Here, injection water is oxygenated, highly purified recycled water produced by advanced water treatment. Injection occurs via a well screened at several depth intervals ranging from 160–365 m, allowing recharge into multiple confined horizons (zones) of the aquifer system. However, these zones are characterized by varying degrees of prior



oxidation due to historic, long-term infiltration from the overlying aquifer. The resulting sediment geochemical heterogeneity provides a critical control on the release (or retention) of arsenic. In zones with prior oxidation, As mobilization occurs via arsenate desorption from Fe-(hydr)oxides, primarily associated with shifts in pH; within zones that remain reduced prior to injection, As release is attributed to the oxidative dissolution of As-bearing pyrite. We find that As release can be attributed to various geochemical mechanisms within a single injection well owing to geochemical heterogeneity across the aquifer system.

■ INTRODUCTION

Managed aquifer recharge (MAR) has become a widely used water management option as it yields many benefits including increased resilience to water supply variability and climate extremes. 1,2 However, recharging water of differing chemical composition than the ambient groundwater will alter the native geochemistry of an aquifer and can cause the mobilization of naturally occurring contaminants. Arsenic is a particular contaminant of concern at MAR sites due to its toxicity to human and ecosystem health and its ubiquity in sediments around the world. Arsenic release is particularly detrimental to MAR if recharge water is to be recovered for potable use. Given a drinking water guideline of 10 μ g L⁻¹,³ even low concentration pulses, on the order of a few μ g L⁻¹, are enough to jeopardize drinking water supplies and render groundwater storage sites unusable without further treatment for As. An understanding of the fundamental geochemical and hydrological processes controlling As mobilization and potential attenuation is critical for determining the scale and longevity of the problem and developing mitigation strategies for protecting groundwater quality.

Various geochemical mechanisms have been observed to cause the release of naturally occurring As from sediments to groundwater during MAR.⁴ Typical causal mechanisms include (i) competitive desorption, (ii) pH-promoted desorption, and (iii) shifts in redox conditions causing the dissolution of As-

bearing minerals and/or reduction of arsenate to arsenite. ^{5–7} Phosphate caused the competitive desorption of arsenic during injection of treated aerated groundwater in The Netherlands. Similarly, As release was attributed to phosphate ligand exchange on Fe-(hydr)oxide surfaces during injection in South Australia. ^{9,10} Increasing pH triggered the desorption of As during infiltration of high quality recharge water in the San Joaquin Valley, California. ¹¹

During the injection of oxygenated water into deep, previously anoxic aquifers, shifting redox conditions control the cycling of arsenic. Arsenic is repartitioned from As-bearing sulfidic minerals (primarily via oxidative dissolution of arsenian pyrite and arsenopyrite) to adsorption sites on freshly precipitated Fe-(hydr)oxide surfaces. The potential for As release then depends on the stability of the surface complexes and host minerals. During aquifer storage and recovery (ASR), groundwater redox conditions can cycle between oxic or suboxic to sulfate reducing conditions causing cyclic repartitioning of

Received: February 8, 2020 Revised: June 3, 2020 Accepted: June 9, 2020 Published: June 9, 2020





arsenic as observed at injection sites in Florida, USA. ^{12–16} At an injection site in The Netherlands, the oxidation of arsenopyrite resulted in formation of Fe-(hydr)oxides but kinetically limited oxidation of dissolved arsenite to arsenate minimized adsorption: a result of the lower binding affinity of arsenite than arsenate for Fe-(hydr)oxides. ¹⁷

Here, we examine As mobilization during MAR via injection of purified, recycled wastewater in Orange County, CA, USA as part of Orange County Water District's (OCWD) Groundwater Replenishment System (GWRS). The GWRS produces potable, high-purity, recycled wastewater which is used for MAR via both infiltration and direct injection into a deep, confined aquifer. Previous work focused on As dynamics during surface infiltration of GWRS water and showed that low concentrations of divalent cations can trigger localized desorption of As(V) oxyanions from phyllosilicate clays. Here, we study the geochemical processes occurring during injection into a deep (>150 m), confined aquifer system via a multiscreened injection well. At this site, different zones of the aquifer are characterized by varying degrees of prior oxidation due to historic, long-term infiltration from the shallow, overlying aquifer.

Constrained by a comprehensive set of field observations, we use 3D reactive transport modeling to understand and analyze the various pathways of As mobilization and immobilization occurring in this vertically heterogeneous aquifer. We demonstrate that As mobilization cannot be attributed to a single causal mechanism but rather to the occurrence of multiple geochemical pathways that dominate As release at different depths within the aquifer system tapped by a single injection well. This study also illustrates how MAR sites can provide unique opportunities to study field-scale As mobility under well-controlled geochemical and hydrological conditions.

MATERIALS AND METHODS

Study Site. Orange County Water District's (OCWD) Groundwater Replenishment System currently operates as the largest advanced treatment facility in the world with a production capacity of 100 million gallons per day (MGD). Recycled wastewater for indirect potable reuse is produced using primary and secondary treatment, followed sequentially by microfiltration, reverse osmosis, advanced oxidation with ultraviolet disinfection, partial decarbonation, and lime addition and is then used for MAR via both infiltration and injection. The recharge water is high purity and highly oxidizing compared to the native groundwater in the injection area (Table 1). In May 2015, OCWD began operating a pilot injection well to assess the feasibility of direct injection into deeper, confined zones of the basin. The injection well is screened at multiple depths, ranging over 161-364 m. Two nested monitoring wells are located 27 and 196 m down gradient from the injection site in Fountain Valley and Santa Ana, CA (Supporting Information, Figures S1 and S2). Monitoring well boreholes were constructed with a rotary drill rig using a reverse-circulation method. The first nested wells (27 m down gradient from injection) are screened at four depth intervals, 179.9-182.9, 210.4-216.5, 243.9-250, and 335.4-339.9 m. The 196 m down gradient well includes three nested monitoring wells, corresponding to depth intervals of 180.5-183.5, 205.8-210.4, and 335.4-338.4 m. The two nested monitoring wells are screened in the same aquifer depths corresponding to screened intervals of the injection well (181.4-184.5, 201.2-216.5, 335.4-341.5 m). Collectively, these monitoring points track water quality evolution within four different hydrostratigraphic units (or zones) of the basin.

Table 1. Average Aqueous Chemistry of Recharge Water and Native Groundwater in the Injection Area

		Native injection area		
Parameter	Recharge water	Zone 1	Zone 2	Zone 3
pН	8.6	7.6	7.5	7.6
Temperature $(^{\circ}C)$	24-29.5 ^a	20.5	20.5	20.5
Dissolved oxygen (mM)	0.1875	0.09	0.094	0
Total organic carbon (mM)	0.0115	0.0196	0.0081	0.0125
As (μM)	0	2.70×10^{-2}	0	2.70×10^{-2}
HCO_3^- (mM)	0.623- 0.705 ^a	3.23	3.23	3.23
CO_3^{2-} (mM)	0.033	< 0.01	< 0.01	< 0.01
Ca^{2+} (mM)	$0.225 - 0.35^a$	1.125	1.125	1.125
$Cl^{-}(mM)$	$0.248 - 0.36^a$	0.44	0.475	0.45
SO_4^{2-} (mM)	5.00×10^{-3}	0.4	0.427	0.468
NO_3^- (mM)	0.129	0.016	0.032	0
PO_4^{3-} (mM)	< 0.0003	0.001	0.0006	0.0003
Depth (m)		161-192	206- 217	344-350
Injection fraction (%)		7.5	38	10
Pyrite $(mg kg^{-1})$		0-516.3	0	716.8
^a Time varying concentrations.				

Injection occurs continuously at approximately 1.5 MGD with slight variations in the injection rate (Supporting Information, Figure S3). Injection has resulted in the mobilization of low concentrations of As (shifting from $\leq 2~\mu g~L^{-1}$ prior to injection and $\leq 8.6~\mu g~L^{-1}$ post injection) from sediments to groundwater. Here, we examine the observed shifts in geochemistry during injection and the causal mechanisms of As release at different depths within the multiaquifer system. We focus on three zones of the multiaquifer system corresponding to depth intervals of 161-192, 206-217, and 344-350 m, with each characterized by distinct geochemical conditions including ambient redox environment and abundance of pyrite and Fe-(hydr)oxides.

Sediment Analysis. Sediment samples were collected from drill cuttings during the installation of a nested monitoring well located 196 m down gradient of the injection well. Drill cuttings were sampled at approximately 1.5 m depth intervals from 161 to 364 m depth and stored at 4 °C. Samples were dried at room temperature, disaggregated by gentle grinding, and analyzed for bulk C and N contents (Carbo Erba CN Elemental Analyzer) and bulk As, Fe, and S contents (Spectro XRF-XEPOS X-ray fluorescence spectrometer). To better characterize the ambient geochemical conditions that prevailed prior to the start of the injection experiment, Fe K-edge extended X-ray absorption fine structure (EXAFS) spectroscopy was conducted to quantify pyrite concentrations for all samples. A subset of sediments containing the highest total As concentrations were further analyzed using As K-edge EXAFS spectroscopy to determine the chemical/mineralogical state of As. While it was not feasible to obtain a continuous anoxic core, this was not expected to impact the total elemental concentrations within the sediments and is taken into account when interpreting solid-phase speciation data. For example, quantified pyrite concentrations in the sediment samples, which had exposure to atmospheric oxygen, were interpreted as a minimum pyrite concentration present in the aquifer.

Aqueous Sampling of Monitoring Wells. Water quality samples were collected and analyzed from monitoring wells approximately every 2 weeks. Field measurements from monitoring wells included dissolved oxygen, pH, and temperature. Collected samples were analyzed for dissolved concentrations of Ca, Fe, Mn, Mg, and Na using inductively coupled plasma atomic emission spectroscopy (ICP AES), EPA Method 200.7. Dissolved total As was measured using inductively coupled plasma mass spectroscopy (ICP MS), EPA Method 200.8. Nitrate was measured by flow injection analysis, Standard Methods 4500NO3-F. Bicarbonate was measured by titration, Standard Method 2320B. Sulfate and chloride were measured by ion chromatography (IC), EPA Method 300.0. 19

Conceptual/Numerical Model of Flow and Nonreactive Transport. Previous site characterization provided an initial, conceptual hydrogeological model and estimates for spatially varying hydraulic conductivities based on aquifer tests, well specific capacity, and lithologic data (Supporting Information, Table S1 and Figure S4). The aquifer section targeted for injection consists of 11 distinct hydrostratigraphic units (also referred to as zones) composed of sand and gravel, separated by lower conductivity silt and clay layers, which were explicitly considered as separate layers. Groundwater flow was dominated by the injection fluxes into the receiving layers with negligible vertical flow across confining layers. The injection volume fraction received in each layer was estimated based on a downhole spinner survey conducted in the injection well. Hydraulic conductivities were calibrated to match observed heads at the monitoring wells. Chloride and temperature were used as intrinsic tracers to calibrate dispersion coefficients and porosities. Both were varying with time in the injection water (temperature showed seasonal variations and chloride varied due to varying influent water quality and treatment processes as shown in Supporting Information, Figures S5 and S6). Groundwater flow and reactive transport models were implemented using MODFLOW²¹ and PHT3D.²² Additional information on model development and calibrated parameters are available in Supporting Information, Table S1. The model simulations focused on three distinct "zones", or hydrostratigraphic units, which exhibit distinct geochemical characteristics. Zone 1 spans a depth of 161-192 m and receives $\sim 7.5\%$ of the injection volume, Zone 2 spans 206-217 m depth and receives \sim 38% of the injection water, and Zone 3 is at a depth interval of 344-350 m and receives ~10% of the injection volume. The remaining injection water recharges units of the aquifer which do not have corresponding monitoring wells and therefore are not further analyzed in this study. Modeling was conducted in 3D under fully transient conditions.

Reaction Network. The reaction network that was employed in this study evolved from previously developed reaction networks for As release and transport at recharge sites in The Netherlands and Florida, USA. Briefly, the main redox process that occurred during injection was the kinetically controlled oxidative dissolution of pyrite by dissolved oxygen and nitrate, simulated as 23-27

$$r_{pyr} = \left[\left(C_{O_2}^{0.5} + C_{NO_3}^{0.5} \right) C_{H^+}^{-0.11} \left(10^{-10.19} \frac{A_{pyr}}{V} \right) \left(\frac{C}{C_o} \right)_{pyr}^{0.67} \right]$$

where C_{O_2} , $C_{NO_3^-}$ and C_{H^+} are the concentrations of dissolved oxygen, nitrate, and protons, respectively. A_{pyr}/V is the ratio of

mineral surface area to solution volume and is taken to be 115 following Wallis et al. (2010); C/C_o is the ratio of pyrite concentration to initial concentration. The release of arsenic results from the kinetic oxidative codissolution of arsenopyrite which is modeled as stoichiometrically linked to the dissolution of pyrite. Initial pyrite concentrations are estimated from the Fe K-edge EXAFS results and calibrated to fit dissolved oxygen and arsenic observations. The stoichiometric ratio is calculated using the molar ratio of pyrite and As. Additional information on input mineral concentrations and expanded modeling methodology is available in Supporting Information, Tables S2 and S3.

In addition to pyrite oxidation, the precipitation of Fe-(hydr)oxides and the subsequent sorption of mobilized As(III) and As(V) onto the Fe-(hydr)oxides was included in the model. The freshly formed Fe-(hydr)oxides were represented as ferrihydrite, and its precipitation was simulated as an equilibrium-controlled process. We include the surface complexation reactions for As(III) and As(V) sorption to ferrihydrite as described in Dzombak and Morel using weak sorption sites with a site density of 0.2 mol mol⁻¹ ferrihydrite and a surface area of 600 m² g^{-1,28} We exclude the competitive adsorption effects of phosphate and carbonate in the implemented reaction network owing to the low or nondetectable concentrations of these species in both the injection water and the monitored groundwater (Table 1). Carbonate concentrations were nondetectable (<0.01 mM) in monitoring well samples for the modeled time period (Supporting Information, Figure S7). Phosphate concentrations in the monitoring wells were generally nondetectable (<0.0003 mM) with small variations reaching a maximum of 0.002 mM (Supporting Information, Figure S8). It was therefore assumed that these species were unlikely to appreciably compete with arsenate for adsorption on Fe-(hydr)oxide surfaces with the arrival of injection water.

Aqueous concentrations in the native groundwater and solid-phase characterization results were used to define the initial conditions prior to the start of injection (Table 1). These conditions varied with depth while being laterally homogeneous. In layers that showed evidence of prior oxidation, solid-phase As was modeled as arsenate adsorbed to ferrihydrite. In initially reduced layers, solid-phase As was modeled as arsenopyrite with initial concentrations corresponding to solid-phase analyses. Arsenite and arsenate were decoupled from the general redox equilibrium as oxidation of As(III) to As(V) was considered kinetically controlled. The inclusion of previously used rates of oxidation of As(III) to As(V) by dissolved oxygen had no effect on simulation results and was therefore not included.

Calcite dissolution was modeled as an equilibrium controlled reaction which buffered pH during injection. Previous geochemical assessments of the site observed the presence of calcite using scanning electron microscopy and found the ambient groundwater to be supersaturated with respect to calcite.²⁹ Initial calcite concentrations in the model were set to ensure an infinite calcite source during the simulation period as described in Supporting Information and shown in Table S2.

Finally, the oxidation of dissolved organic matter by various electron acceptors was also considered, assumed to occur locally during injection, and modeled following a commonly employed Monod-type rate expression

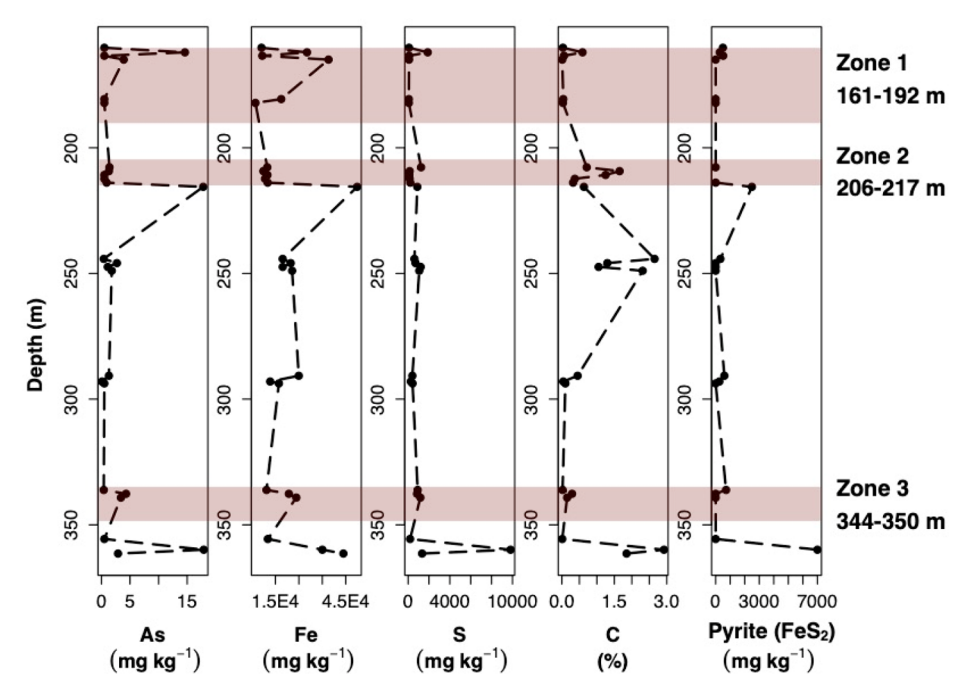


Figure 1. Bulk solid-phase concentrations of As $(mg kg^{-1})$, Fe $(mg kg^{-1})$, S $(mg kg^{-1})$, total C (%) as determined using XRF (As, Fe, S), elemental analyzer (C), and pyrite concentrations quantified using EXAFS.

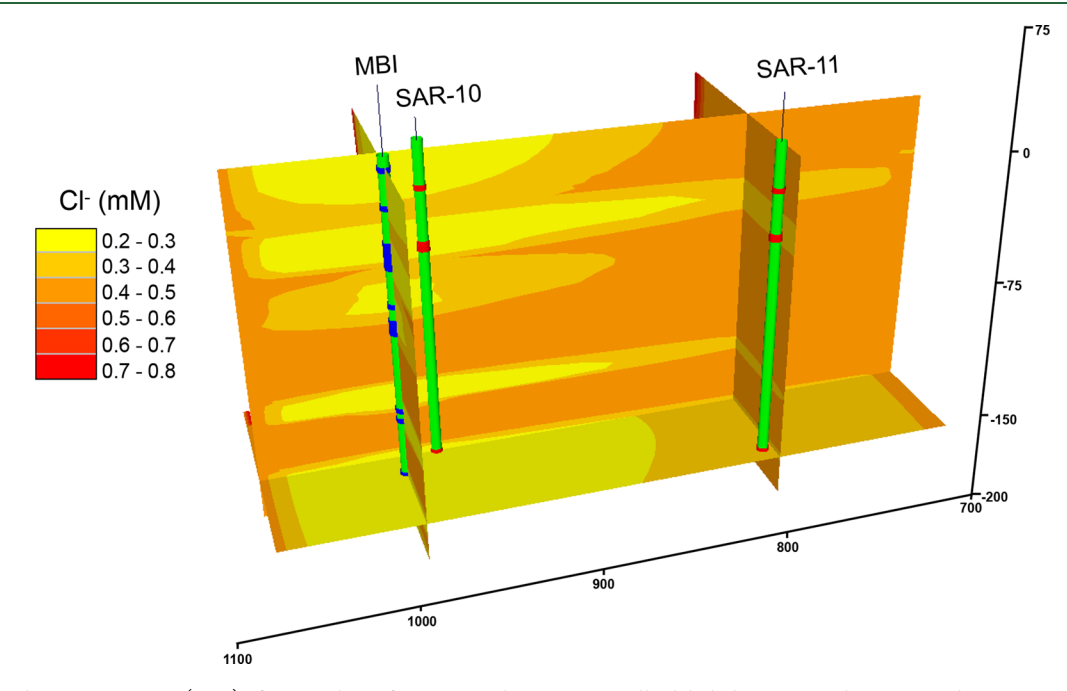


Figure 2. Chloride concentrations (mM) after 238 days of injection. The injection well is labeled as MBI, and SAR-10 and SAR-11 represent 27 m and 196 m down gradient monitoring wells, respectively. Blue zones on MBI well indicate screened injection intervals while red zones on SAR-10 and SAR-11 indicate screened monitoring depth intervals.

$$r_{DOC} = \left[k_{O_2} \frac{C_{O_2}}{2.94 \times 10^{-4} + C_{O_2}} + k_{NO_3} \frac{C_{NO_3^-}}{1.55 \times 10^{-4} + C_{NO_3^-}} + k_{SO_4^2 -} \frac{C_{SO_4^{2-}}}{1.0 \times 10^{-4} + C_{SO_4^{2-}}} \right]$$

where $k_{\rm O_2}$, $k_{\rm NO_3}^-$, $k_{\rm SO_4^{2-}}$ are rate constants for aerobic, denitrifying, and sulfate-reducing conditions and are equivalent to 1.57 \times 10⁻⁹, 1.67 \times 10⁻¹¹, and 1 \times 10⁻¹³ mol L⁻¹ s⁻¹, respectively, as reported in Prommer and Stuyfzand.²⁴ $C_{\rm O_2}$,

 $C_{{
m NO_3}^-}$ and $C_{{
m SO_4}^{2-}}$ are groundwater concentrations of DO, nitrate, and sulfate.

RESULTS

Sediment Analysis and Native Aquifer Geochemistry.

Sediments collected from the aquifer zones that are targeted by injection show strata with relatively high concentrations of redox sensitive species, including As, Fe, and S (Figure 1). Concentrations of As are comparable with global averages in sediments (3–10 mg kg⁻¹ As)⁶ with a maximum of 17.9 mg

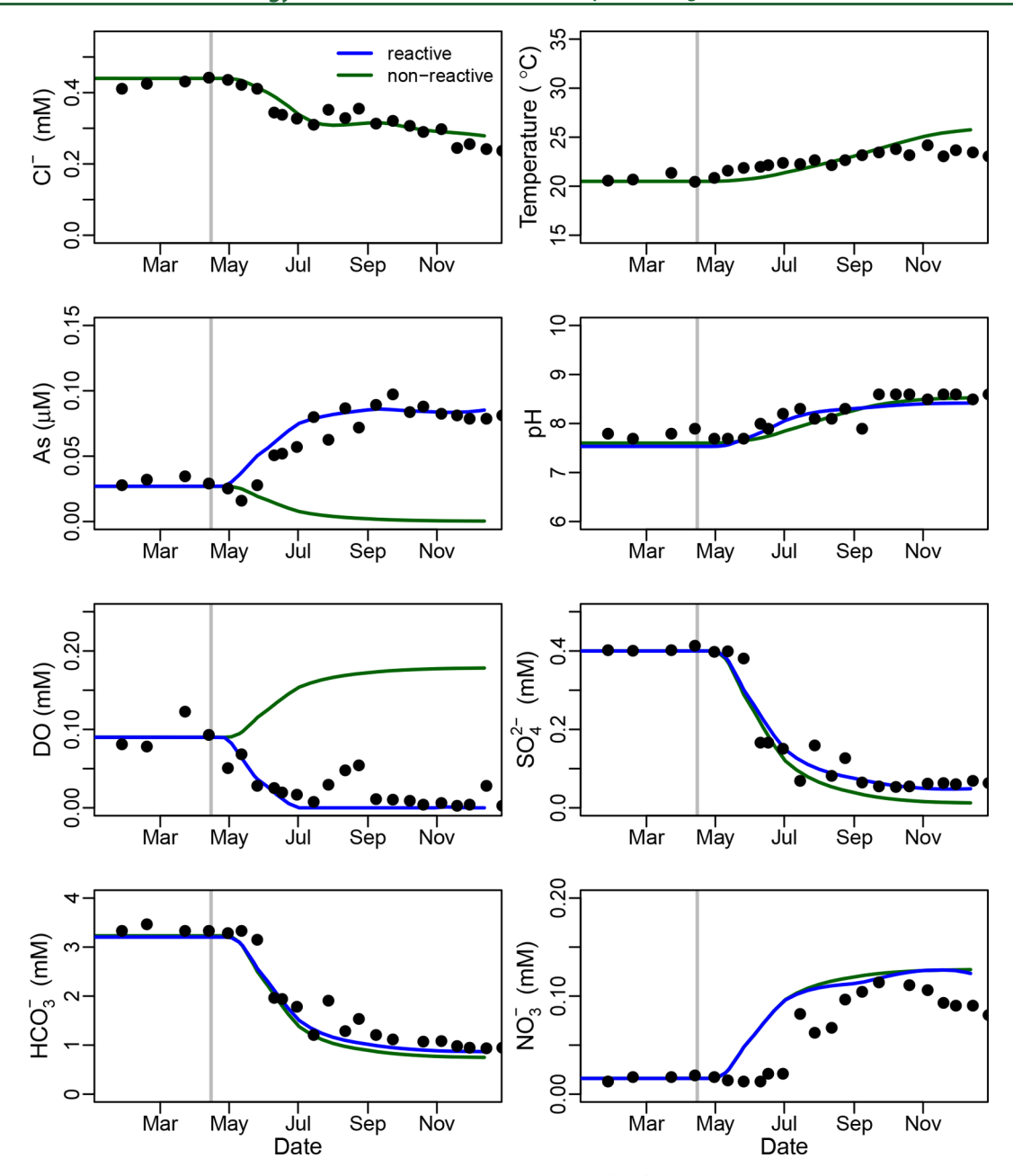


Figure 3. Observed and modeled changes in groundwater concentration of total As (μM) , pH, dissolved oxygen, sulfate, bicarbonate, and nitrate (mM) in Zone 1 (161-192 m) at a monitoring well located 27 m down gradient from the injection well. Blue lines represent reactive model simulation while green lines show nonreactive behavior for comparison. The vertical gray line represents the beginning of injection.

kg⁻¹. Although sediments were not collected anoxically, pyrite was observed in several strata, coinciding with the presence of elevated concentrations of bulk As, Fe and S in the sediments (Figure 1) and other redox sensitive elements including U, V, Mn, N (Supporting Information, S9). Additionally, As K-edge EXAFS confirmed the persistence of As-bearing sulfidic minerals (data not shown); sediments collected from a depth of approximately 162 m showed approximately 29% of total arsenic residing as arsenopyrite, indicating that a considerable fraction of As resides as arsenopyrite under native aquifer conditions.

Zone 1 spans a large depth interval, and elevated pyrite concentrations (reaching up to 498 mg kg⁻¹ FeS₂) reside in the top of the zone directly in the uppermost injection screened interval (161.6-164.6 m), while monitoring well locations are positioned deeper within the zone (179.9-182.9 m); see

Figure 2. Surprisingly, groundwater from the monitoring well in Zone 1 showed a background concentration of dissolved oxygen ($\sim 0.1~\text{mM})$ prior to injection (Figure 3). However, this finding is consistent with solid-phase data which together suggests that an oxidized portion of the zone persists below a reduced portion. Zone 2 has no detectable pyrite with solid-phase As concentrations below 2 mg kg $^{-1}$ (Figure 4) and an initial background DO concentration of approximately 0.1 mM. Pyrite concentrations in Zone 3 reach 716.8 mg kg $^{-1}$ in the injection interval depth and at monitoring well depths with limited initial DO (<0.02 mM) in the native groundwater (Figure 5).

Nonreactive Tracers. Prior to examining the geochemical processes controlling As mobilization, we focus on interpreting the observed changes in water chemistry between the injection well and monitoring well SAR-10 located 27 m down gradient, i.e., the shifts in water chemistry within several days of the start

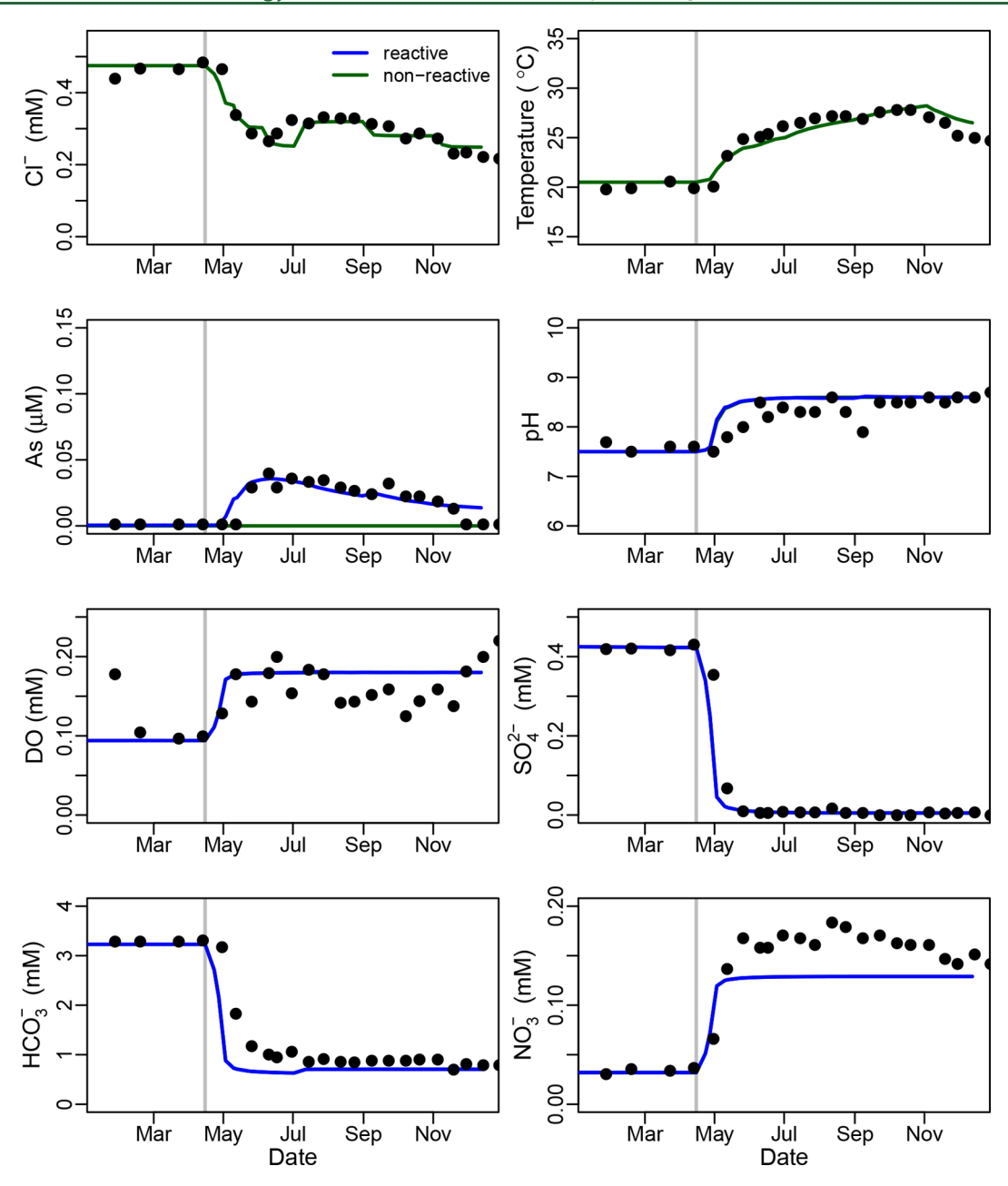


Figure 4. Observed and modeled changes in groundwater concentration of total As (μM) , pH, dissolved oxygen, sulfate, bicarbonate and nitrate (mM) in Zone 2 (206-217 m) at a monitoring well located 27 m down gradient from the injection well. Blue lines represent reactive model simulation while green lines show nonreactive behavior for comparison. The vertical gray line represents the beginning of injection. For pH, DO, SO_4^{2-} , HCO_3^{-} , and NO_3^{-} , nonreactive lines are overlapped by reactive lines indicating these species behave conservatively in this Zone.

of injection (Figure 2). In addition to examining Cl⁻, we use field-observed temperatures as an intrinsic tracer to more reliably constrain the flow and physical transport behavior.

A rapid decrease in Cl⁻ concentration is observed in all zones, signaling the arrival of high-purity injection water (Figures 3–5). Additionally, groundwater temperature increases with the seasonally varying but continuously warmer, injection water (Figures 3–5). We focus on simulated and observed data in the 27 m down gradient monitoring well; the 196 m down gradient well only begun to receive injection water at the time of the analysis. The calibrated model replicates the observations from the 196 m down gradient well (see Figures S10–S12). However, there is greater discrepancy between simulated and observed concentrations at the 196 m down gradient well compared to the 27 m down gradient well. This is attributed to the increased

impact of lateral heterogeneity at farther distances away from the injection well as shown by geophysical logs (Supporting Information, Figure S4). The lithologies of the injection well and 27 m down gradient well are more similar compared to that of the 196 m down gradient well. The simplifying assumption of lateral homogeneity is less valid at farther distances from the injection well.

Injection-Induced Redox Shift and Arsenic Mobilization. The heterogeneity in native geochemistry results in varying reaction mechanisms upon injection of the recharge water. Zone 1 represents a hydrostratigraphic unit that is partially oxidized. Although initial DO concentrations are lower (~0.1 mM) than those in the injection water (~0.2 mM), the DO concentrations at the monitoring wells decline in response to injection (Figure 3). Although the monitoring well resides in

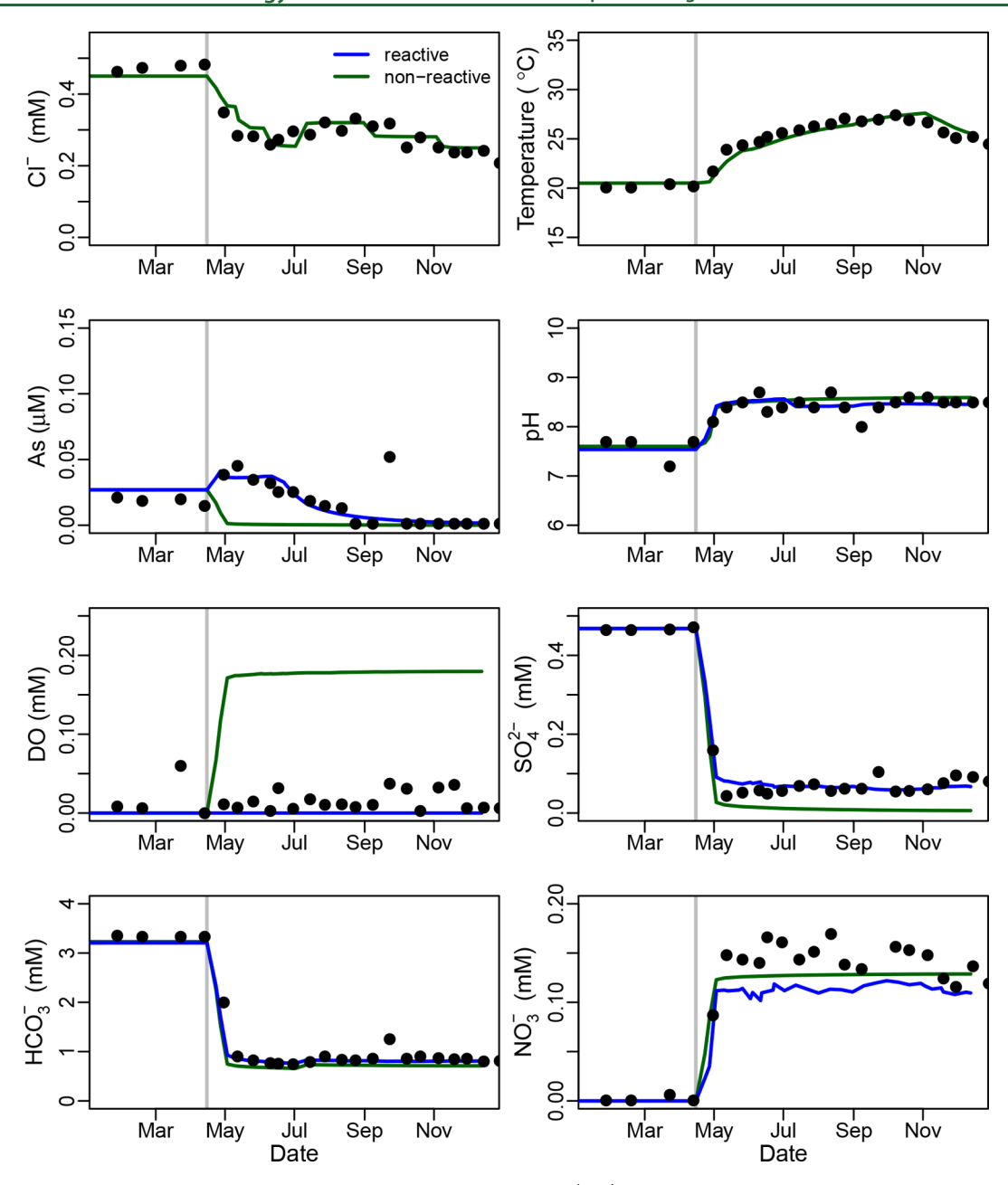


Figure 5. Observed and modeled changes in groundwater concentration of total As (μM) , pH, dissolved oxygen, sulfate, bicarbonate and nitrate (mM) in Zone 3 (344-350 m) at a monitoring well located 27 m down gradient from the injection well. Blue lines represent reactive model simulation while green lines show nonreactive behavior for comparison. The vertical gray line represents the beginning of injection.

an oxidized region within the zone, the injection well is screened above a reduced aquifer section containing As-bearing pyrite and dissolved organic carbon (schematic representation in Supporting Information, Figure S13). Injection results in vertical displacement of anoxic water above and toward the monitoring well below. In the injection area of Zone 1, DO declines while As increases; we capture these changes by considering the DO consumption by As-bearing pyrite and dissolved organic carbon. The oxidation of pyritic minerals also results in the release and observed increase in total arsenic. Sulfate is significantly flushed out due to the low ($<0.5 \text{ mg L}^{-1}$) sulfate concentrations in the injection water. However, observed sulfate concentrations are higher than those obtained by the nonreactive simulations (Figure 3) owing to the oxidation of pyritic minerals and the associated release of sulfate (Figure 3). While the pH of the injectant is high (\sim 8.6) relative to the native

groundwater, the oxidation of pyrite and organic matter causes a decrease in pH. Our simulations are only able to reproduce the observed pH increase that occurred despite the presence of pyrite oxidation by including a pH buffering process. For this site, calcite dissolution was assumed to act as the key buffering mechanism, similar to a number of other MAR sites. Other pH buffering processes of minor importance at this site may include proton buffering or the dissolution of alumninosilicates. Aluminosilicate dissolution was excluded from the reaction network owing to the slower rates of aluminosilicate dissolution in comparison to calcite dissolution at circumneutral pH. Similarly, laboratory-scale experiments using sediments from an MAR site found that pH buffering by calcite dissolution was dominant relative to aluminosilicate dissolution. While calcium concentrations were measured and modeled, it was difficult to use these concentrations as strong constraints for

calcite dissolution rates owing to the less frequent sampling of dissolved calcium (Supporting Information, Figure S14). Zone 1 showed approximately 0.1 mmol per liter bulk volume (mol $L_{\rm B}^{-1}$) dissolution of calcite (Supporting Information, Figure S15). The assumption of equilibrium with calcite and the kinetically controlled oxidation of organic carbon together provides strong agreement with the measured ${\rm HCO_3}^-$ concentrations. Increasing the rate of nitrate reduction that is attributed to pyrite and/or organic carbon only decreases the magnitude of the post breakthrough nitrate concentrations, but it does not reproduce the field-observed lag in nitrate breakthrough.

In the case of Zone 2, solid-phase analysis and the preinjection aqueous chemical composition suggest that extensive oxidation has occurred prior to injection (Figure 4). After the onset of injection, DO concentrations increase and stabilize at the injectant concentration. Given that conservative transport simulations for sulfate, HCO₃-, pH, and DO match the fieldobserved breakthrough behavior, this indicates that the groundwater chemistry is dictated by the injectant composition rather than the sediment geochemistry. Simulated solid-phase arsenate concentrations were limited to the As sorbed to Fe-(hydr)oxides that prevail in that zone. The observed, temporary increase in dissolved arsenate concentrations coincides with an increase in pH and a transient peak, which is well matched by the model simulations. Arsenic concentrations subsequently decline after the pH-promoted desorption of a labile fraction of As previously adsorbed on Fe-(hydr)oxides. Nitrate concentrations are underestimated in our simulations, and observed values are higher than the injectant concentration indicating nitrate production within the aquifer. Although the injection water contains a limited concentration of ammonia/ammonium $(\sim 0.02 \text{ mM})$, the simulation of ammonia/ammonium oxidation could not reproduce the observed nitrate concentrations without consumption of dissolved oxygen, which was not observed.

Finally, Zone 3 represents a horizon of the aquifer that is initially anoxic (DO levels are below detection), with pyrite and arsenopyrite residing at the same depths as the injection and monitoring well screens. Dissolved oxygen remained low following injection, indicating the consumption of oxygen during the migration of the injectant (Figure 5). As with Zone 1, to capture the observed consumption of oxygen, we allow pyrite and arsenopyrite oxidation to proceed, which produces sulfate concentrations consistent with observation and higher than the corresponding nonreactive simulations, which are unable to reproduce the measured concentrations. The increase and subsequent decline of dissolved arsenic concentrations is simulated by the oxidation of a finite, rapidly depleting initial concentration of arsenic-bearing pyritic minerals, consistent with the measured low solid-phase concentration of arsenic in the sediments ($<4 \text{ mg kg}^{-1}$). Additionally, the acidity-producing oxidation of pyrite requires the presence of calcite dissolution in order to simulate the observed groundwater pH. Zone 3 showed approximately 0.5 mmol L_B⁻¹ dissolution of calcite (Supporting Information, Figure S15). The greater dissolution of calcite in Zone 3 is likely attributed to this Zone receiving a larger fraction of injection water over a smaller zone thickness relative to Zone 1. Similar to Zone 2, breakthrough of NO₃⁻ is underestimated, again suggesting that a source (inclusive of a generation process) of NO₃ is present, which is not accounted for in the current reaction network.

DISCUSSION

Mechanisms of As Mobilization. Our combined measurements and reactive transport simulations indicate how strongly geochemical heterogeneity can impact water quality evolution during artificial recharge.³⁴ In the case of the Orange County Groundwater Basin, both partially oxidized and reduced zones of the aquifer are being simultaneously targeted for injection. The heterogeneity in redox state exists due to historic, long-term exposure to oxidized water infiltrating from the overlying shallow aquifer. As a result, multiple geochemical mechanisms of arsenic release and mobilization are operative within a single injection well, resulting in spatially heterogeneous As concentrations and also differences in the longevity of the As release.

In previously reduced portions of the aquifer (Figures 3 and 5), the introduction of oxygenated water causes the repartitioning of As from reduced As-bearing pyritic minerals to freshly precipitated Fe-(hydr)oxides. Rather than the induction of an increase in dissolved arsenic concentrations, a repartitioning process between solid phases occurs. Thereafter, dissolved concentrations of As are controlled by the binding of arsenate on Fe(III)-(hydr)oxides. The adsorbed and steadily accumulating arsenate is therefore vulnerable to shifts in pH above ~8.5 and also to the onset of anaerobic/reducing conditions or the introduction of competing ligands (e.g., phosphate). Decreasing or eliminating the supply of oxygenated injection water could reverse redox condition to a reducing environment and potentially cause the reductive dissolution of As(V)-bearing Fe(III)-(hydr)oxides; the combined outcome could cause an increase in As concentrations, as previously observed at ASR sites in Florida. 16 Additionally, in these reduced zones, the adsorption of As to Fe-(hydr)oxides is limited due to the increasing groundwater pH caused by calcite dissolution.

In contrast, in the oxidized aquifer zones (Figure 4), arsenic initially resides as arsenate bound to Fe(III)-(hydr)oxides. Although the injection of oxygenated water does not affect the redox conditions within the previously oxidized zone, the mobilization similarly depends on the stability of As(V) on Fe(III)-(hydr)oxides complexes; the onset of reducing conditions or pH increases above 8.5 could liberate large amounts of As.

In the case of Orange County, the increase in groundwater pH during injection to values above 8 results in arsenate desorption and concomitant increases in dissolved concentrations. Once the fraction of labile arsenate bound to Fe-(hydr)oxides is depleted, As release will cease and concentrations will decrease to below background levels. However, in the oxidized zone, pH increases are not attributed to calcite dissolution but rather are controlled by the higher pH of the injectant water.

Behavior of Other Trace Elements. Arsenic poses the largest threat to groundwater quality compared to the observed total dissolved concentrations of Zn, Ni, Co, Cu, Mn, V, and Cr (Supporting Information, Figures S16–S21) and owing to its low regulatory limit. Cobalt and copper were nondetectable in all samples. Zinc concentrations fluctuated at low levels (<0.1 μ mol L⁻¹) before and after injection and did not show clear trends with the arrival of recharge water. Similarly, initial background concentrations of chromium were either nondetectable or low (<0.06 μ mol L⁻¹) and generally fell below detection after injection. The trends in V concentration are similar to that of As with a larger magnitude (reaching approximately 5.9 μ mol L⁻¹). Similar to the initial release of As, vanadium is likely liberated to solution by oxidative

dissolution processes occurring with the arrival of injection water. While V is not currently regulated in the USA, future regulation could have compliance implications for MAR sites.

Implications for Groundwater Management. A common management strategy during MAR is to use a recharge water chemistry that closely resembles native groundwater. However, we demonstrate that geochemical heterogeneity can pose a complex challenge for water managers seeking to minimize or inhibit metals release and mobilization during MAR. In the case of geochemical heterogeneity within the target aquifer, the native water cannot be uniformly replicated, and it can be challenging to determine a single recharge water composition that inhibits As mobilization across all aquifer zones.

Possibly the largest threat of arsenic mobilization comes from the risk of shifting redox conditions, particularly from oxidizing (aerated) to reducing conditions. In oxygenated environments, arsenic, if present, is typically hosted by Fe(III)-(hydr)oxides that can become subject to reductive dissolution, and liberation of As, upon the onset of reducing conditions. At our study site, both oxidized and reduced sediments receive the same injectant water composition. In previously oxidized systems, the introduction of oxygenated water will have no effect on redox chemistry if the water is also void of reductants such as labile dissolved organic carbon or ammonium. To prevent the onset of reducing conditions and subsequent As mobilization, the most cautious action is to maintain these aquifer zones at continuously oxic conditions.

However, although oxygenated water will preserve conditions that limit arsenate desorption in oxic zones, it will cause the oxidative dissolution of As-bearing pyritic minerals in the reduced zones of the aquifer. In previously reduced aquifers, adjusting injectant chemistry to remove residual oxidants from the recharged water may limit As release via oxidative dissolution of As-bearing pyritic materials. At a recharge site in Florida, the removal of oxidants (including DO and residual disinfectants such as chloramines and hydrogen peroxide) from the treated recharge water via membrane contactors and sodium bisulfide addition was used to decrease As mobilization in receiving aquifers.³⁵ Similarly, the deoxygenation of injectant was found to significantly lower arsenic concentrations at a (re)injection site in southeast Queensland, Australia. 36 Within the Orange County Groundwater Basin, injection of oxidants (primarily DO) leads to a short-pulse of arsenic before reattenuation on sediment minerals, likely freshly formed Fe(III)-(hydr)oxides. Thus, a shift in solid-phase partitioning occurs but with no lasting impacts on dissolved arsenic concentrations, which remain low. However, after repartitioning from As-bearing sulfides to Fe(III)-(hydr)oxides, dissolved arsenic concentrations are largely regulated by pH.

In both previously oxidized and reduced aquifer zones of the injection area, it is therefore critical to maintain pH values below 8.5 to limit pH-promoted desorption from Fe-(hydr)oxides, which are either previously abundant in oxidized zones or freshly formed during oxidation of reduced zones. When pH-promoted desorption occurs, potential mitigation can involve adjusting the final pH of the treated recharge water to values matching the native groundwater.³⁶ However, when sediment interactions control groundwater pH (e.g., via calcite dissolution, acidity produced by pyrite and/or organic matter oxidation), pH adjustments to the injectant will have limited effect or must be adjusted aggressively to counteract geochemical reactions influencing pH. The feasibility of using pH adjustment as a

method to minimize As mobilization will depend on the pH buffering capacity of the sediments, which is additionally a function of recharge volume and rates: both of which can potentially be adjusted; a high buffering capacity can be offset by a greater injection rate and/or more acidic injectant. Alternatively, when groundwater pH is controlled by calcite dissolution, a more effective approach can involve increasing calcium concentrations to increase the saturation of recharge water with respect to calcite and limit dissolution of carbonate and subsequent increase in groundwater pH. While pHpromoted desorption is the dominant control on arsenic mobilization at our field site, the significance of these processes and efficacy of the management approaches described above will depend on various site-specific geochemical conditions including the ionic composition of the surrounding groundwater which influences the surface complexation of arsenic on Fe-(hydr)oxide surfaces. Additionally, operational, site-specific constraints may affect the feasibility of these management strategies. For example, the lower pH increases the corrosion potential of injectate waters with some commonly used transmission pipeline and injection well materials. Where sitespecific reactive transport models exist, the feasibility of treatment options and mitigation strategies can be assessed, compared, and optimized through predictive modeling.

This work highlights the importance and complexity of site-specific heterogeneity in geochemical conditions causing shifts in groundwater quality during MAR. Historical groundwater usage can cause variations in geochemical conditions that affect MAR operations. Accordingly, it is important to comprehensively characterize target aquifers, consider the history of aquifers, as well as the resulting geochemical conditions in addition to natural geochemical heterogeneity, and design site-specific management strategies aimed at limiting mobilization of As from multiple release processes during artificial recharge.

ASSOCIATED CONTENT

Supporting Information

The Supporting Information is available free of charge at https://pubs.acs.org/doi/10.1021/acs.est.0c00794.

Detailed modeling methodology, map of injection area, schematic of injection and monitoring well locations, simulated and observed aqueous concentrations for 196 m down gradient monitoring well, conceptual schematic of geochemical conditions in the aquifer zones, expanded description of the reactive transport model, additional solid-phase concentrations, and monitoring well data for additional aqueous species (PDF)

AUTHOR INFORMATION

Corresponding Author

Scott Fendorf — Department of Earth System Science, Stanford University, Stanford, California 94305, United States; orcid.org/0000-0002-9177-1809; Phone: 650-723-5238; Email: fendorf@stanford.edu

Authors

Sarah Fakhreddine — Department of Earth System Science, Stanford University, Stanford, California 94305, United States Henning Prommer — CSIRO Land and Water, Wembley, WA 6913, Australia; School of Earth Sciences, University of Western Australia, Crawley, Western Australia 6913, Australia; orcid.org/0000-0002-8669-8184 Steven M. Gorelick — Department of Earth System Science, Stanford University, Stanford, California 94305, United States Jason Dadakis — Orange County Water District, Fountain Valley, California 92708, United States

Complete contact information is available at: https://pubs.acs.org/10.1021/acs.est.0c00794

Notes

The authors declare no competing financial interest.

ACKNOWLEDGMENTS

We are grateful to Donald Phipps and Megan Plumlee (Orange County Water District) for providing geochemical data and support. We thank Doug Kent, Massimo Rolle, David Freyberg, and Kate Maher for valuable input and discussion; and Guangchao Li, Doug Turner, and Juan Lezama Pacheco for their analytical assistance. Use of the Stanford Synchrotron Radiation Lightsource, SLAC National Accelerator Laboratory, is supported by the U.S. Department of Energy, Office of Science, Office of Basic Energy Sciences. We thank the Stanford Research Computing Center for providing computational resources and support. The effort of Steven Gorelick was supported in part by the National Science Foundation under grant ICER/EAR-1829999 to Stanford University as part of the Belmont Forum - Sustainable Urbanisation Global Initiative (SUGI)/ Food-Water-Energy Nexus theme. Any opinions, findings, conclusions, or recommendations expressed in this material are those of the authors and do not necessarily reflect the views of the National Science Foundation.

REFERENCES

- (1) Perrone, D.; Merri Rohde, M. Benefits and Economic Costs of Managed Aquifer Recharge in California. San Franc. Estuary Watershed Sci. 2016, 14 (2). DOI: 10.15447/sfews.2016v14iss2art4
- (2) Scanlon, B. R.; Reedy, R. C.; Faunt, C. C.; Pool, D.; Uhlman, K. Enhancing Drought Resilience with Conjunctive Use and Managed Aquifer Recharge in California and Arizona. *Environ. Res. Lett.* **2016**, *11* (3), 035013.
- (3) WHO. Guidelines for Drinking-Water Quality: First Addendum to Vol. 1, Recommendations; World Health Organization, 2006.
- (4) Neil, C. W.; Yang, Y. J.; Jun, Y.-S. Arsenic Mobilization and Attenuation by Mineral—Water Interactions: Implications for Managed Aquifer Recharge. *J. Environ. Monit.* **2012**, *14* (7), 1772—1788.
- (5) Cullen, W. R.; Reimer, K. J. Arsenic Speciation in the Environment. *Chem. Rev.* **1989**, 89 (4), 713–764.
- (6) Smith, E.; Naidu, R.; Alston, A. M. Arsenic in the Soil Environment: A Review. Adv. Agron. 1998, 64, 149–195.
- (7) Smedley, P. L.; Kinniburgh, D. G. A Review of the Source, Behaviour and Distribution of Arsenic in Natural Waters. *Appl. Geochem.* **2002**, *17* (5), 517–568.
- (8) Appelo, C. a. J.; Vet, W. W. J. M. de. Modeling in Situ Iron Removal from Groundwater with Trace Elements Such as As. In *Arsenic in Ground Water*; Springer, Boston, MA, 2003; pp 381–401. DOI: 10.1007/0-306-47956-7 14.
- (9) Vanderzalm, J. L.; Page, D. W.; Barry, K. E.; Scheiderich, K.; Gonzalez, D.; Dillon, P. J. Probabilistic Approach to Evaluation of Metal(Loid) Fate During Stormwater Aquifer Storage and Recovery. Clean: Soil, Air, Water 2016, 44 (12), 1672–1684.
- (10) Vanderzalm, J. L.; Dillon, P. J.; Barry, K. E.; Miotlinski, K.; Kirby, J. K.; Le Gal La Salle, C. Arsenic Mobility and Impact on Recovered Water Quality during Aquifer Storage and Recovery Using Reclaimed Water in a Carbonate Aquifer. *Appl. Geochem.* **2011**, *26* (12), 1946–1955
- (11) McNab, W. W.; Singleton, M. J.; Moran, J. E.; Esser, B. K. Ion Exchange and Trace Element Surface Complexation Reactions

- Associated with Applied Recharge of Low-TDS Water in the San Joaquin Valley, California. *Appl. Geochem.* **2009**, 24 (1), 129–137.
- (12) Jones, G. W.; Pichler, T. Relationship between Pyrite Stability and Arsenic Mobility During Aquifer Storage and Recovery in Southwest Central Florida. *Environ. Sci. Technol.* **2007**, *41* (3), 723–730.
- (13) Mirecki, J. E. Geochemical Models of Water-Quality Changes During Aquifer Storage Recovery (ASR) Cycle Tests, Phase 1: Geochemical Models Using Existing Data; ERDC/EL-TR-06-8; Engineer Research and Development Center, 2006.
- (14) Mirecki, J. E.; Bennett, M. W.; López-Baláez, M. C. Arsenic Control during Aquifer Storage Recovery Cycle Tests in the Floridan Aquifer. *Groundwater* **2012**, *51* (4), 539–549.
- (15) Price, R. E.; Pichler, T. Abundance and Mineralogical Association of Arsenic in the Suwannee Limestone (Florida): Implications for Arsenic Release during Water–Rock Interaction. *Chem. Geol.* **2006**, 228 (1–3), 44–56.
- (16) Wallis, I.; Prommer, H.; Pichler, T.; Post, V.; Norton, B. S.; Annable, M. D.; Simmons, C. T. Process-Based Reactive Transport Model To Quantify Arsenic Mobility during Aquifer Storage and Recovery of Potable Water. *Environ. Sci. Technol.* **2011**, *45* (16), 6924–6931.
- (17) Wallis, I.; Prommer, H.; Simmons, C. T.; Post, V.; Stuyfzand, P. J. Evaluation of Conceptual and Numerical Models for Arsenic Mobilization and Attenuation during Managed Aquifer Recharge. *Environ. Sci. Technol.* **2010**, *44* (13), 5035–5041.
- (18) Fakhreddine, S.; Dittmar, J.; Phipps, D.; Dadakis, J.; Fendorf, S. Geochemical Triggers of Arsenic Mobilization During Managed Aquifer Recharge. *Environ. Sci. Technol.* **2015**. 497802.
- (19) US EPA. Methods for the Determination of Chemical Substances in Marine and Estuarine Environmental Samples; US Environmental Protection Agency: Cincinnati, OH, 1992.
- (20) APHA; AWWA; WEF. Standard Methods for the Examination of Water and Wastewater, 22nd ed.; American Public Health Association, American Water Works Association, Water Environment Federation, 2012.
- (21) Harbaugh, A. W.; Banta, E. R.; Hill, M. C.; McDonald, M. G. MODFLOW-2000, The U.S. Geological Survey Modular Ground-Water Model User Guide to Modularization Concepts and the Ground-Water Flow Process; OFR-2000—92; United States Geological Survey, 2000.
- (22) Prommer, H.; Barry, D. A.; Zheng, C. MODFLOW/MT3DMS-Based Reactive Multicomponent Transport Modeling. *Groundwater* **2003**, 41 (2).247
- (23) Descourvieres, C.; Prommer, H.; Oldham, C.; Greskowiak, J.; Hartog, N. Kinetic Reaction Modeling Framework for Identifying and Quantifying Reductant Reactivity in Heterogeneous Aquifer Sediments. *Environ. Sci. Technol.* **2010**, 44 (17), 6698–6705.
- (24) Prommer, H.; Stuyfzand, P. J. Identification of Temperature-Dependent Water Quality Changes during a Deep Well Injection Experiment in a Pyritic Aquifer. *Environ. Sci. Technol.* **2005**, 39 (7), 2200–2209.
- (25) Rathi, B.; Siade, A. J.; Donn, M. J.; Helm, L.; Morris, R.; Davis, J. A.; Berg, M.; Prommer, H. Multiscale Characterization and Quantification of Arsenic Mobilization and Attenuation During Injection of Treated Coal Seam Gas Coproduced Water into Deep Aquifers. *Water Resour. Res.* 2017, 53 (12), 10779–10801.
- (26) Seibert, S.; Atteia, O.; Ursula Salmon, S.; Siade, A.; Douglas, G.; Prommer, H. Identification and Quantification of Redox and PH Buffering Processes in a Heterogeneous, Low Carbonate Aquifer during Managed Aquifer Recharge. *Water Resour. Res.* **2016**, 52 (5), 4003–4025
- (27) Williamson, M. A.; Rimstidt, J. D. The Kinetics and Electrochemical Rate-Determining Step of Aqueous Pyrite Oxidation. *Geochim. Cosmochim. Acta* 1994, 58 (24), 5443–5454.
- (28) Dzombak, D. A.; Morel, F. M. M. Surface Complexation Modeling: Hydrous Ferric Oxide; Wiley, New York, 1990.
- (29) MWH. Demonstration Mid-Basin Injection Well Project; Well Completion Report; Prepared for Orange County Water District, 2013.

- (30) Greskowiak, J.; Prommer, H.; Massmann, G.; Nützmann, G. Modeling Seasonal Redox Dynamics and the Corresponding Fate of the Pharmaceutical Residue Phenazone During Artificial Recharge of Groundwater. *Environ. Sci. Technol.* **2006**, 40 (21), 6615–6621.
- (31) Greskowiak, J.; Prommer, H.; Vanderzalm, J.; Pavelic, P.; Dillon, P. Modeling of Carbon Cycling and Biogeochemical Changes during Injection and Recovery of Reclaimed Water at Bolivar. *Water Resour. Res.* 2005, 41 (10), W10418.
- (32) Stuyfzand, P. J. Quality Changes upon Injection into Anoxic Aquifers in the Netherlands: Evaluation of 11 Experiments. *Artif. Recharge Groundwater* **1998**, 283–291.
- (33) Rozalén, M. L.; Huertas, F. J.; Brady, P. V.; Cama, J.; García-Palma, S.; Linares, J. Experimental Study of the Effect of PH on the Kinetics of Montmorillonite Dissolution at 25°C. *Geochim. Cosmochim. Acta* **2008**, *72* (17), 4224–4253.
- (34) Descourvières, C.; Hartog, N.; Patterson, B. M.; Oldham, C.; Prommer, H. Geochemical Controls on Sediment Reactivity and Buffering Processes in a Heterogeneous Aquifer. *Appl. Geochem.* **2010**, 25 (2), 261–275.
- (35) MacNevin, D.; Mercer, T.; Bennett, J.; Fahey, R.; Moore, E.; Kinslow, J. Groundwater Replenishment Performance and Operations: Lessons Learned During Clearwater's One-Year Pilot; Orlando, FL, 2015.
- (36) Prommer, H.; Sun, J.; Helm, L.; Rathi, B.; Siade, A. J.; Morris, R. Deoxygenation Prevents Arsenic Mobilization during Deepwell Injection into Sulfide-Bearing Aquifers. *Environ. Sci. Technol.* **2018**, 52 (23), 13801–13810.